ARTICLE

Spherical and rod shaped mesoporous nanosilicas for cancer-targeted and photosensitizers delivery in photodynamic therapy

Received 00th January 20xx,
Accepted 00th January 20xx

DOI: 10.1039/d1tb02299g

Wioleta Borzęcka,[abc] Patrícia M. R. Pereira,[ad] Rosa Fernandes,*[de] Tito Trindade,*[b] Tomás Torres*[cfg] and João P. C. Tomé*[ah]

Mesoporous silica nanoparticles (MSNPs) have attracted much attention in many biomedical applications. One of the fields in which smart functional nanosystems have found wide application is in cancer treatment. Here, we present new silica nanoparticle-based systems which have been explored as efficient vehicles to transport and deliver photosensitizers (PSs) into tumor tissues during photodynamic therapy (PDT). In this work, we report the preparation, characterization and, *in vitro* studies of distinct shaped MSNPs grafted with *S*-glycoside porphyrins (Pors). The ensuing nanomaterials were fully characterized, and their properties as third-generation PSs for PDT against two bladder cancer cell lines, HT-1376 and UM-UC-3, were examined. The best uptake results were obtained for **MSNP-PS2**, while **MSNP-PS1** showed the lowest cellular uptake among the nanocarriers tested, but revealed the best phototoxicity in both cancer cells. Overall, the phototoxicity was higher with MSNPs than with mesoporous silica nanorods (MSNRs) and higher uptake and phototoxicity were consistently observed in UM-UC-3 rather than in HT-1376 cancer cells.

1. Introduction

Among the new treatments developed for bladder cancer, photodynamic therapy (PDT) has shown promising survival rates, which increases the relevance of research on this therapy for this clinical condition.[1] PDT combines three components: drug, light and oxygen, which by their own do not have any toxic effects on the biological systems. However, strong cytotoxic is observed in the target cells when reactive oxygen species (ROS) are produced while the drug (PS) is in contact with molecular oxygen and exposed to light with an appropriate wavelength.[2] As PS molecules do not show toxicity until activated by light irradiation, systemic side effects can be easily avoided in PDT compared to other cancer therapies.[3]

PDT with Photofrin was first approved for bladder cancer treatment 27 years ago in Canada.[4] Although many years past since then, PDT still has limitations as a general protocol for treating different types of cancer. Some of those limitations are related to the clinical use of PS, namely: 1) low generation of singlet oxygen production ($^1O_2$) due to the hydrophobic character of the most used PS; 2) many PSs exhibit a non-specific biodistribution and poor selectivity for tumor tissue over normal tissues, which can lead to prolonged skin sensitivity; 3) the lifetime of $^1O_2$ limits its diffusion to more or less 10 to 55 nm in cells making PDT a selective treatment but, unfortunately, its effectiveness also decreases with tissue thickness.[3, 5] In this context, nanoparticles have emerged as promising vehicles for PS used in PDT, thus opening a new possibility to improve this therapy in bladder cancer treatment.[6] The application of PSs nanoformulations in PDT can enhance the treatment by increasing the biocompatibility of hydrophobic PS and their blood circulation. Moreover, NPs can accumulate and remain selectively, in tumor tissues due to enhanced permeability and retention effect (EPR) -mediated passive tumor targeting.[7]

In the early 1990s, a new family of molecular sieves was discovered which are often called M41S.[8] In 2001, J. Perez-Pariente *et al.*[9] used for the first time MCM-41 as a host in a drug delivery system containing ibuprofen molecules as the guests. They reported that ibuprofen molecules occupied part of the MCM-41 mesopores and could diffuse out of the host by placing the loaded samples in a simulated body fluid. This led to

[a.] *QOPNA-LAQV-REQUINTE and Department of Chemistry, University of Aveiro, 3810-193 Aveiro, Portugal*
[b.] *CICECO-Aveiro Institute of Materials and Department of Chemistry, University of Aveiro, 3810-193 Aveiro, Portugal*
[c.] *Department of Organic Chemistry, Autonoma University of Madrid, 28049 Madrid, Spain*
[d.] *Coimbra Institute for Clinical and Biomedical Research (iCBR), Faculty of Medicine, University of Coimbra, Azinhaga de Santa Comba, 3000-548 Coimbra, Portugal*
[e.] *Center for Innovative Biomedicine and Biotechnology (CIBB), University of Coimbra, 3004-531 Coimbra, Portugal*
[f.] *IMDEA-Nanociencia, Campus de Cantoblanco, c/Faraday 9, 28049 Madrid, Spain*
[g.] *Institute for Advanced Research in Chemical Sciences (IAdChem), Universidad Autónoma de Madrid (UAM), 28049 Madrid, Spain*
[h.] *Centro de Química Estrutural & Departamento de Engenharia Química, Instituto Superior Técnico, Universidade de Lisboa, 1049-001 Lisboa, Portugal; e-mail: jtome@tecnico.ulisboa.pt*

† Footnotes relating to the title and/or authors should appear here.
Electronic Supplementary Information (ESI) available: [details of any supplementary information available should be included here]. See DOI: 10.1039/x0xx00000x

new studies on the use of silica nanoparticles (SNPs) as drug delivery systems[10] and since then, mesoporous silica materials have been explored and investigated for biomedical applications. MSNPs have attracted wide attention for PDT owing to their biocompatibility, large surface area per volume ratio, controllable size formation, hydrophilic surface, and ability for surface functionalization.[11] The possibility of using these systems for tumor targeting through adequate surface modification is a key to successful cancer treatment.[12] Currently, there are different Food and Drug Administration (FDA)-approved nanoparticle-based drug delivery systems and others are under clinical trials.[13]

Different parameters, including particle size distribution, shape, and surface chemistry play an important role in the biocompatibility and uptake efficiency of MSNPs.[14] While these parameters have been studied extensively in recent years, data concerning their role is still limited because there is a lack of consistency in the reported literature.[12] For instance, based on current literature it is difficult to deduce that rod-shaped silica NPs are better for passive targeting than traditional spherical NPs. This difficulty may be related to the fact that the results obtained in silica-based NPs are conflicting with other NPs with different compositions.[12] For example, B. D. Chithrani *at. al.*[15] have reported that Au nanospheres showed better uptake in HeLa cells than rod-shaped NPs. On the other hand, Florez *et. al.*[16] observed a cell type independent correlation between the increase of aspect ratio and decrease of NPs uptake when investigating polymeric NPs in MSC and HeLa cells. Y. Zhang and coworkers[17] reported that the cellular uptake of three-dimensional spherical polystyrene NPs was higher than two-dimensional disk polystyrene NPs in HeLa, Hek 293, and BJ cells. On the other hand, changing polystyrene NPs from a spherical to a disk shape promotes their cell surface binding. Furthermore, Y. Huang *et. al.*[18] designed three types of MSNPs with different aspect ratios: 1 (100 x 100 nm), 2 (240 x 100 nm), 4 (450 x 100 nm) while maintaining a similar chemical composition. They concluded that NPs with larger aspect ratios were taken up in larger amounts and had faster internalization rates in A375 cells. Among the NP investigated by the authors, rod-like NPs with longer longitudinal axis provide a larger contact area with the cell membrane, which might explain the results. The same tendency was observed by the group of Yang *et. al.*.[19] Compared to spherical NPs, NPs with a larger aspect ratio showed much faster uptake by 4T1 murine breast cancer cells. Also, Meng et. al.[20] investigated the cellular uptake efficiencies of three rod-like MSNP samples characterized by distinct aspect ratios: 1.5-1.7 (110-130 x 60-80 nm), 2.1-2.5 (160-190 x 60-90 nm), and 4-4.5 (260-300 x 50-70 nm), using HeLa and A549 cancer cell line. The cells showed faster uptake for the MSNPs with intermediate aspect ratios (2.1-2.5) and also in larger quantities as compared to the shorter or longer rod lengths. Y. Yang and Y. Chengzhong[12] suggested that one possible explanation for this inconsistency could be the fact that separating one parameter of NPs and at the same time keeping all the other parameters unchanging to study the behavior of NPs is challenging.

Recent studies have demonstrated that grafting Pors inside or over the surfaces of MSNPs could limit the formation of Pors aggregates, increase their water compatibility and decrease the pre-mature release of Pors. Hence, the use of MSNPs as PS carriers can enhance the selectivity of Pors for targeted tissues and consequently increase the PDT efficiency.[21 22 23 24 25 26] Recently, we have reported the enhancement of PDT for bladder cancer by using glycosylated Pors as PS encapsulated in amorphous SiO_2 nanospheres.[27]

Encouraged by these results and considering that the morphology of SiO_2 NPs could affect both the biodistribution and cellular uptake[12, 14, 28] we decided to investigate the effect of particle shape using the same Pors attached to spherical and rod-like MSNPs. To the best of our knowledge, this is the first time that the behavior of spherical and rod-like MSNPs grafted with S-glycoside Pors is assessed by *in vitro* experiments performed with bladder cancer cells. For this purpose, different MSNPs bearing *S*-glycoside Pors were prepared. As a model PS 5,10,15,20-tetrakis(pentafluorophenyl)porphyrin ($TPPF_{20}$, **PS0**, **Figure 1**) was chosen. For cancer cells targeting, 5,10,15,20-tetrakis(4-1'-thio-glucosyl-2,3,5,6-tetrafluorophenyl)porphyrin (SGlc-Por, **PS1**, **Figure 1**) and 5,10,15,20-tetrakis(4-1'-thio-galactosyl-2,3,5,6-tetrafluorophenyl)porphyrin (SGal-Por, **PS2**, **Figure 1**) were investigated. These two PSs bear, respectively, glucose and galactose moieties which are crucial for tumor targeting. Since galectin[29] and glucose[29b, 30] binding proteins are expressed in high levels in cancer cells it is important to design PSs with glycol-molecules to obtain successful cancer treatment by precise tumor targeting. Thus, **PS1** and **PS2** were grafted on the surface of MSNPs using the synthetic strategy presented in **Scheme 1**. HT-1376 and UM-UC-3 bladder cancer cell lines, derived from transitional cell carcinoma, were chosen as models because both have different affinities for galactose and glucose derivatives. Both cells express glycobinding proteins but in different levels: glucose transporter (GLUT1) and galactose-binding protein (galectin-1).[29b] Moreover, in order to compare the silica particles' shape-dependent behavior in HT-1376 and UM-UC-3 cancer cell lines, sphere-shaped MSNPs and rod-shaped mesoporous silica nanorods (MSNRs) were prepared in this research. Finally, the *in vitro* photodynamic efficacy of the new nanomaterials was undertaken on HT-1376 and UM-UC-3 bladder cancer cells.

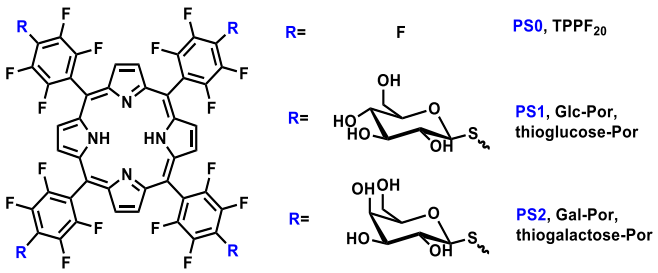

Figure 1. Structures of PS0, PS1 and PS2.

2. Experimental

General methods

Absorption spectra were recorded using a JASCO V-660 UV-Visible Spectrophotometer. FT-IR spectra were recorded in KBr pellets using GRASEBY SPECAC or with Cary 630 FT-IR Spectrometer. The irradiation system used to determine the production of $^1O_2$ was the Newport irradiation system, consisting of a 300 W halogen lamp, FSQ-OG530 color glass filter for wavelengths <530 nm, and magnetic stirrer. The irradiation system used to determine the phototoxicity during biological experiments was a Lumacare system, model LC-122, consisting of a 250 W halogen lamp coupled to an optical fiber (with a cutoff filter for wavelengths <540 nm). The radiation power was measured with a potentiometer bright Spectra Physics, model 407A, and the sensor of the same brand, model 407A-2. Transmission electron microscopy (TEM) images were obtained using a JEOL JEM1010 transmission electron microscope operating at an acceleration voltage of 100 kV.

All reagents were obtained from commercial sources and were used without further purification steps. Reverse phase column chromatography was carried out on Waters Sep-Pak C18 35 cm^3 cartridges. Analytical thin layer chromatography (TLC) was carried out on pre-coated silica gel sheets (Merck, 60, 0.2 mm).

Synthesis of NPs

Synthesis of MSNPs and MSNRs

MSNPs and **MSNRs** were prepared after slight modification of the method presented in the literature.[31] In a first step, CTAB (100 mg, 2.74 mM for **MSNP-100**, 200 mg, 5.49 mM, for **MSNP-200**, 400 mg, 10.98 mM for **MSNP-400**, 500 mg, 13.72 mM for **MSNP-500**,) was dissolved in water (100 mL) in Erlenmeyer flask equipped with magnetic bar. Next, to the above solution ethyl acetate (0.88 mL) and NH_4OH (30%, 2.7 mL) were subsequently added. In the end, TEOS (500 µL, 2.24 mmol) was added and the solution was stirred for 5 min at RT. After that, 100 mL of water was added to slower the hydrolysis of TEOS and accelerates the silica condensation. After 24 h of stirring at RT, NPs were filtered and washed with EtOH. To remove the surfactant templates, nanoparticles were redispersed in 100 mL of ethanol/acetic acid (glacial) mixture (95/5, v/v) and the mixture was stirred for 30 minutes. In the end, nanoparticles were washed with EtOH and air-dried.

MSNPs' and MSNRs' functionalization with APTS

To the suspension of 30 mg of **MSNPs** or **MSNRs** in 2.5 mL H_2O, 158 µL of APTS in 750 µL of EtOH was added. After adjusting the pH to 7 by adding 0.2 M HCl (2.25 mL) the reaction was stirred at RT for 24 h. **MSNPs-NH_2** and **MSNRs-NH_2** were washed with EtOH and air-dried.

Grafting of PS on the surface of MSNPs-NH_2 and MSNRs-NH_2

The grafting of porphyrins **PS0**, **PS1**, and **PS2** on the nanomaterials **MSNPs-NH_2** and **MSNRs-NH_2** were carried out in DMSO at 160 °C according to the literature, with minor modifications.[32] 35 mg of **MSNPs-NH_2** or **MSNPs-NH_2** were resuspended in DMSO (1 mL). A solution of **PS** (2.38 µmol) in DMSO (4 mL) was added to that suspension and the resulting mixture was magnetically stirred for 96 h at 160 °C. After that time, red hybrid materials were obtained. The resulting hybrid materials were washed with DMSO and EtOH until no Soret and Q bands were observed in the rinse solvent and air-dried. The amount of unreacted porphyrin was calculated by UV-Vis spectrophotometry.

Singlet oxygen generation study

Singlet oxygen ($^1O_2$) was determined by a chemical method using 1,3-diphenylisobenzofuran (DPBF). DPBF has an absorption maximum at 415 nm, thus it is possible to follow the ability of the NPs to generate $^1O_2$ by measuring the DPBF absorption decay, at this wavelength.

The solutions were irradiated at RT under magnetic stirring and light from a 300 W halogen lamp with a cutoff filter for wavelengths <530 nm (**Figure SI 2**). 5,10,15,20-tetrakis-phenyl-21,23-H-porphyrin (**TPP**) was used as a reference compound. **TPP** (0.5 µM), **PS0** (0.5 µM), **PS1** (0.5 µM), **PS2** (0.5 µM), **MSNP-PS0** (0.5 µM, 2.5 µM of PS), **MSNP-PS1** (0.5 µM, 2.5 µM of PS), **MSNP-PS2** (0.5 µM, 2.5 µM of PS), **MSNR-PS1** (2.5 µM of PS) or **MSNR-PS2** (2.5 µM of PS) were placed into 3 mL cuvette which contained DMSO. Then DPBF (50 µM) in DMSO was added (total volume in cuvette 3 mL). The final solutions were irradiated at RT and under gentle magnetic stirring and light from a 300 W halogen lamp (with a cut off filter for wavelengths <530 nm). The breakdown of DPBF was monitored by measuring the decrease in absorbance at 415 nm at pre-established irradiation intervals. The results were expressed by plotting the DPBF depletion against the irradiation time. The depletion of DPBF was calculated as follows: $DPBF\ depletion = Abs_1/Abs_0$. Abs_0 and Abs_1 are the absorbance values at 415 nm before and after irradiation, respectively.

***In vitro* assays**

Cells culture

Human bladder cancer cell lines UM-UC-3 and HT-1376 derived from high-grade transitional cell carcinoma were obtained from the American Type Culture Collection (ATCC®, Manassas, VA, USA). Cells were cultured in Roswell Park Memorial Institute (RPMI)-1640 medium (Sigma) supplemented with 2 $g.L^{-1}$ sodium bicarbonate (Sigma), 2 mM L-glutamine (Sigma), 10% (v/v) of heat-inactivated Fetal Bovine Serum (FBS; Life Technologies, Carlsbad, CA, USA) and antibiotic/antimicotic containing 100 units.mL-1 penicillin, 100 µg.mL-1 streptomycin and 0.25 µg.mL-1 amphotericin B (Sigma). UM-UC-3 and HT-1376 cells were seeded at a density of 1.5 x 104 in 96-well culture plates (Orange Scientific, Braine-l'Alleud, Belgium). 24 hours after plating, cells were overnight incubated with different concentrations of NPs (0-20 µM of PS in RPMI medium) in the dark.

Cellular uptake of NPs

After incubation with NPs in the dark, UM-UC-3 and HT-1376 cells were washed with PBS buffer and mechanically scrapped in 1% (m/v) sodium dodecyl sulfate (SDS; Sigma) in PBS buffer at pH 7.0. NPs intracellular concentration was determined by spectrofluorimetry using a microplate reader (Synergy HT, Biotek, Winooski, VT, USA) with the excitation filter (set at

360±40 nm) and emission filter (645±40 nm). Results were normalized for protein concentration (determined by bicinchoninic acid reagent; Pierce, Rockford, IL, USA).

PDT treatments on cells

Photodynamic irradiation was carried out in a fresh culture medium, in the absence of NPs, covering UM-UC-3 and HT-1376 cell monolayers with RPMI medium and exposing them to white light delivered by the illumination system LC-122 LumaCare at 8.4 mW/cm^{-2} for 40 min. As a control, sham-irradiated cells were used. These cells were kept in the dark for the same durations and under the same conditions as the irradiated cells. In all trials, triplicate wells were settled under each experimental condition, and each experiment was repeated at least three times.

MTT assay

MTT assay was used to determine cell metabolic activity after NPs incubation in the dark, irradiation, or both after 24 h. This colorimetric assay is measuring the ability of bladder cancer cells to reduce yellow 3-[4,5-dimethylthiazol-2-yl]-2,5-diphenyl-tetrazolium bromide (MTT, Sigma), to a purple formazan on a microplate reader (Synergy HT). The results are expressed in percentage of control (i.e. optical density of formazan from cells not exposed to NPs).

Statistical analysis

Statistical data analysis was carried out using Excel's Analysis ToolPak (Student's t test). The values are represented as mean ± s.e.m. Level of significance was set at values *P<0.05,**P<0.01 and ***P<0.001.

Results and discussion

Preparation and characterization of MSNPs and MSNRs

MSNPs and MSNRs have been prepared under alkaline conditions using tetraethoxysilane (TEOS) as the silica precursor and cetyltrimethylammonium bromide (CTAB) as the structure directing agent.[31] In a first approach, the sample **MSNP-PS0** was prepared (**Scheme 1**) and then evaluated for $^1O_2$ generation in *in vitro* studies using two human bladder cancer cell lines, HT-1376 and UM-UC-3. These experiments using **MSNP-PS0** allowed a preliminary assessment of this type of MSNPs and, based on the results obtained, other samples with better cancer cells recognition have been prepared. Thus, nanomaterials bearing PS with sugar moieties (**MSNP-PS1**, **MSNP-PS2**, **MSNR-PS1**, **MSNR-PS2**) were prepared (**Scheme 1**) and fully characterized. For that purpose, **PS1** and **PS2** were synthesized according to literature procedures described elsewhere.[33] Mesoporous silicas with distinct aspect ratios were obtained by varying the amount of CTAB (2.74 mM for **MSNP-100**, 5.49 mM for **MSNP-200**, 10.98 mM for **MSNP-400**, 13.72 mM for **MSNP-500**, **Table 1**) dissolved in the reacting mixture. In this reaction, CTAB serves as an organic template for the formation of mesoporous silica frameworks.

The average size of the NPs was estimated by transmission electron microscopy (TEM) after dispersing the sample in water and drying it at ambient temperature. (**Figure 2, Table 1**).

Table 1 indicates that the shape of the particles depends on the CTAB concentration used in the synthesis of mesoporous silicas. Hence, the higher the concentration of CTAB in the reaction mixture, the higher the aspect ratio (length:width) of the particles, which is in agreement with previous reports.[18, 34] To compare shape-dependent behavior in HT-1376 and UM-UC-3 cancer cell lines, sphere-shaped **MSNP-100** (117 ± 16 nm) and rod-shaped **MSNR-500** (175 ± 39 nm x 36 ± 7 nm) were chosen and named, respectively as **MSNP** and **MSNR**. **Figure -2** shows the TEM images of samples **MSNP** and **MSNR** selected for further studies.

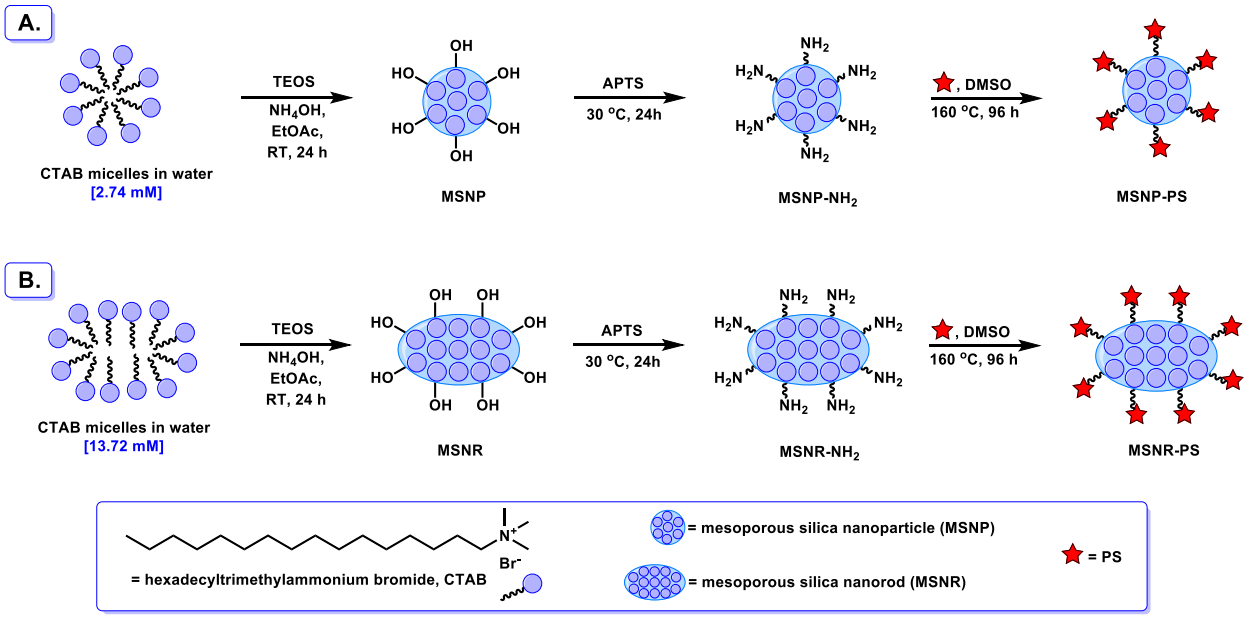

Scheme 1. Schematic preparation of the hybrid nanomaterials grafted with PSs showing the difference between the preparation of MSNP (A) and MSNR (B).

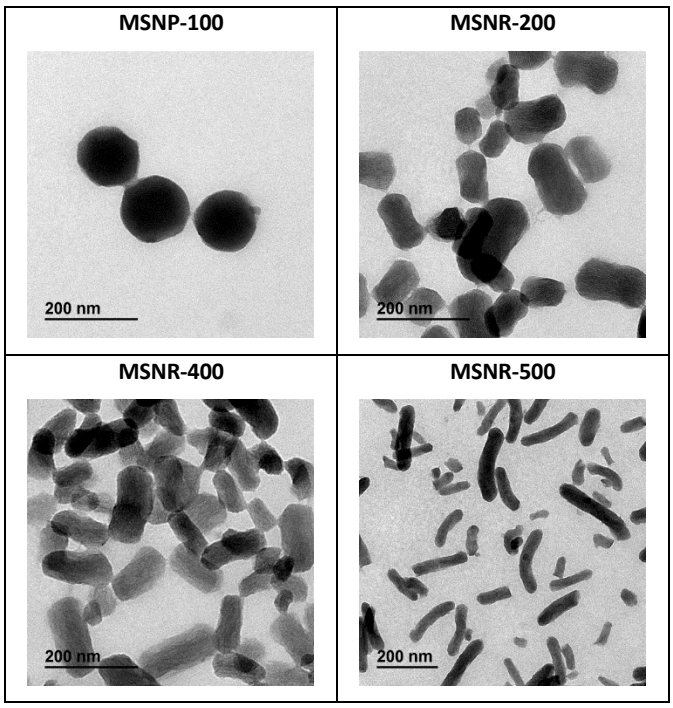

Figure 2. TEM images of **MSNP-100**, **MSNR-200**, **MSNR-400** and **MSNR-500**.

Table 1. Size of NPs estimated from TEM. Information on mean size and standard deviation was calculated from measuring more than 100 NPs in random fields of TEM grids. *NPs used as cores for further experiments.

Nanomaterial name	CTAB [mg /mM]	NPs'		Aspect ratio (length: width)
		length [nm]	width [nm]	
MSNP-100*	100/2.74	117 ± 16	117 ± 16	1
MSNR-200	200/5.49	125 ± 32	65 ± 11	1.9
MSNR-400	400/10.98	134 ± 25	57 ± 12	2.4
MSNR-500*	500/13.72	175 ± 39	36 ± 7	4.9

The PSs molecules were covalently bound onto the surfaces of MSNPs and MSNRs using (3-aminopropyl)triethoxysilane (APTS) as the molecular linker. Firstly, MSNPs and MSNRs were functionalized with APTS by dispersing the NPs in water and then adding a solution of APTS in ethanol to produce mesoporous silicas with amine terminal groups at the surfaces (**MSNPs-NH_2** and **MSNRs-NH_2**). In the last step of the preparation, the grafting of Por: **PS0**, **PS1**, and **PS2** on the surface of **MSNPs-NH_2** and **MSNRs-NH_2** was carried out in DMSO at 160 °C.[32, 35] The final hybrid materials were washed with DMSO and EtOH until the typical Soret and Q bands of Pors were not observed in the rinsed solvent. The amount of Por covalently attached to NPs was calculated using UV-Vis spectrophotometry by subtracting the unreacted Por (from the rinse solvent) from Por taken into the reaction mixture. The highest amount of PS in the mesoporous silica samples was observed for **MSNP-PS0** (26.4 nmol/mg, **Table 2**), which could be explained by the fact that **PS0** is not bearing any sugar molecules. Thus, **PS0** has the higher reactive para-fluorine atoms, which allows easier conjugation with nanomaterials compare to **PS1** and **PS2**.

Table 2. Concentration of PS on the surface of NP.

Starting nanomaterial name	PS	Final nanomaterial name	Concentration of PS in the NP [nmol of PS/mg of NP]
MSNP-100	**PS 0**	**MSNP-PS0**	26.4
MSNP-100	**PS 1**	**MSNP-PS1**	25.0
MSNP-100	**PS 2**	**MSNP-PS2**	19.8
MSNR-500	**PS 1**	**MSNR-PS1**	22.9
MSNR-500	**PS 2**	**MSNR-PS2**	22.6

The UV-VIS absorption spectra of all PSs and their nanoformulations were collected after dissolving and dispersing the samples in DMSO, respectively (**Figures SI 3-5**). Pors presented Soret bands at 417 nm (**PS0**) and 421 nm (**PS1** and **PS2**). Furthermore, all NPs showed the typical spectra of a free base Por, with Soret bands at 436 nm (**MSNP-PS0**), 431 nm (**MSNP-PS1**), 435 nm (**MSNP-PS2**), 436 nm (**MSNR-PS1**), and 438 nm (**MSNR-PS2**).

The FT-IR was used to evaluate the functionalization of MSNPs and MSNRs with APTS (**Figure SI 6**) and further covalent bonding with Pors (**Figure SI 7-9**). The aminated NPs exhibited the presence of the N–H bending band at ~1600 cm^{-1} and broad bands in 2800 to 3800 cm^{-1} region, corresponding to stretching vibrations of primary amines, which indicated that the amino groups were bound onto the NPs surface.[36] After covalent functionalization with Pors, a new band appeared at ~1590 cm^{-1} corresponding to the C=C vibrational modes of Pors. The band at ~1700 cm^{-1} could be attributed to the bending vibration of the C=N of the Por ring.

Singlet oxygen generation study

The ability of the functionalized nanomaterials to generate $^1O_2$ was determined by an indirect chemical method in which 1,3-diphenylisobenzofuran (DPBF) acts as a $^1O_2$ quencher. DPBF has an absorption maximum at 415 nm and forms a colorless endoperoxide product when it reacts with singlet oxygen (**Figure SI 1**). In this method, the ability of PSs or NPs to generate $^1O_2$ is measured by following the DPBF absorption decay at its maximum absorption (415 nm).

In this study, all solutions or suspensions for analysis were prepared in DMSO and stirred under irradiation for defined time intervals, at room temperature. Probes were exposed to the light of a 300 W halogen lamp. Incident light was filtered through an orange filter to take out light below 530 nm. Tetraphenylporphyrin (TPP) was used as a reference compound. Under these conditions, all MSNPs and MSNRs tested were photostable (**Table SI 1**).

The $^1O_2$ generation was determined for all nanoformulations (**MSNP-PS0**, **MSNP-PS1**, **MSNR-PS1**, **MSNP-PS2**, **MSNR-PS2**) and the corresponding PSs (**PS0**, **PS1,** and **PS2**) (**Figure 3**). The free **PS0**, **PS1**, and **PS2** were tested at concentrations of 0.5 µM and new nanomaterials were tested at concentrations of PS: 0.5 µM and 2.5 µM. Free **PS 1** and **PS 2** oxidized DPBF in the same

way. **PS0** oxidized DPBF slightly less than PSs bearing sugar moieties.

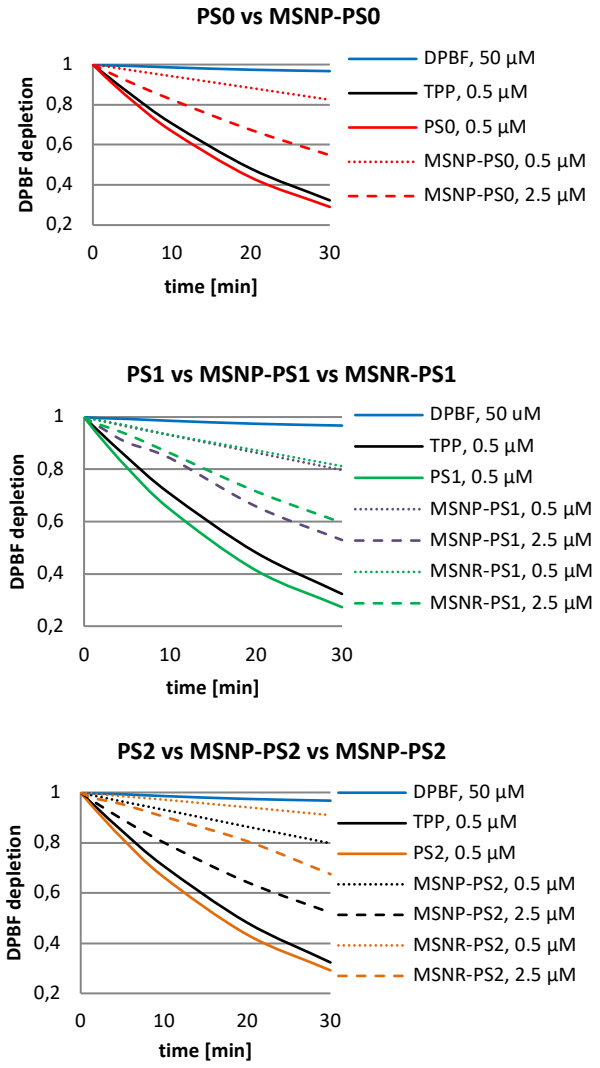

Figure 3. $^1O_2$ generation by **PS0**, **PS1**, **PS2** and its corresponding NPs (**MSNP-PS0, MSNP-PS1, MSNP-PS2** and **MSNR-PS1, MSNR-PS2**) where each point represents the mean of at least three independent experiments and has a standard deviation lower than 3 %. Concentrations indicated for all nanomaterials refer to the equivalent concentration of non-immobilized porphyrins.

From the $^1O_2$ generation study, we could observe that free **PS0**, **PS1**, and **PS2** oxidized DPBF almost in the same way (**Figure 4**). DPBF kinetic decay was similar in all sphere-shaped particles (**MSNP-PS0, MSNP-PS1, MSNP-PS2**). After 30 min of irradiation, these nanoformulations were able to reduce about 50% of DPBF with 2.5 µM of PS concentration. All sphere-shaped particles produced more $^1O_2$ than rod-shaped particles (**Figure 4**), suggesting that MSNPs could be more efficient than MSNRs in terms of cancer treatment in PDT. This could be due to the fact that in smaller NPs (NPs with smaller size aspect ratio, **Table 1**), there is a higher surface area. Thus, our MSNPs are more effective in $^1O_2$ production than MSNRs, under equal experimental conditions.

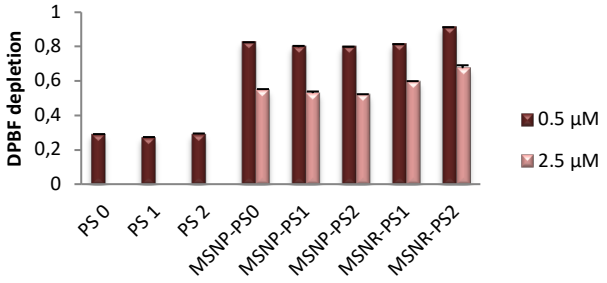

Figure 4. DPBF depletion in the presence of **PS0**, **PS1**, **PS2** and its corresponding NPs (**MSNP-PS0, MSNP-PS1, MSNP-PS2**, and **MSNR-PS1, MSNR-PS2**) at different concentrations (0.5 and 2.5 µM) after 30 min of irradiation. Concentrations indicated for all nanomaterials refer to the equivalent concentration of non-immobilized Pors. Data are the mean value of at least three independent experiments and have a standard deviation lower than 3 %.

In vitro studies

In vitro studies were carried out into two human bladder cancer cell lines, HT-1376 and UM-UC-3. These cell lines express the glyco-binding proteins (glucose transporter, GLUT1 and the galactose-binding protein, galectin-1) in different levels,[29b] which have a key role in the uptake and phototoxicity of galactodendritic porphyrinoids.[29b] GLUT1 is expressed at higher levels in HT-1376 cancer cells than in UM-UC-3 cells, whereas galectin-1 is expressed at higher levels in UM-UC-3 cells than in HT-1376 cells.[29b]

Cellular uptake of PSs and their nanoformulations

Preliminary uptake studies were performed using free PS (**PS0**, **PS1**, **PS2**). Bladder cancer cells were incubated in dark conditions with increasing concentrations of PS (2.5, 5, 10 µM prepared in PBS, maximum 0.5% DMSO v/v) for 4 h. Fluorescence spectroscopy studies demonstrated that **PS1** accumulation was higher in HT-1376 than in UM-UC-3 cancer cells (**Figure 5**). On the other hand, the uptake of **PS0** and **PS2** was higher in UM-UC-3 than in HT-1376 cancer cells. The use of porphyrins with sugar moieties demonstrated higher uptake when compared with **PS0**, suggesting the sugar-tumor binding in cells expressing GLUT-1 and galectin-1. In the case of the bioconjugates **PS1** and **PS2**, the uptake was dependent on the concentration of the PS and cell line. Among the studied PSs, the highest uptake was observed for **PS1**. For 10 µM of gluco-**PS1**, the intracellular accumulation was almost twice in both cancer cell lines compared to galacto-**PS2**. This could be caused by the fact that both HT-1376 and UM-UC-3 cancer cells have higher levels of glucose receptors when compared with galactose receptors.[33a] Thus, the presence of sugar moieties is important during the uptake of PSs by both cancer cells.

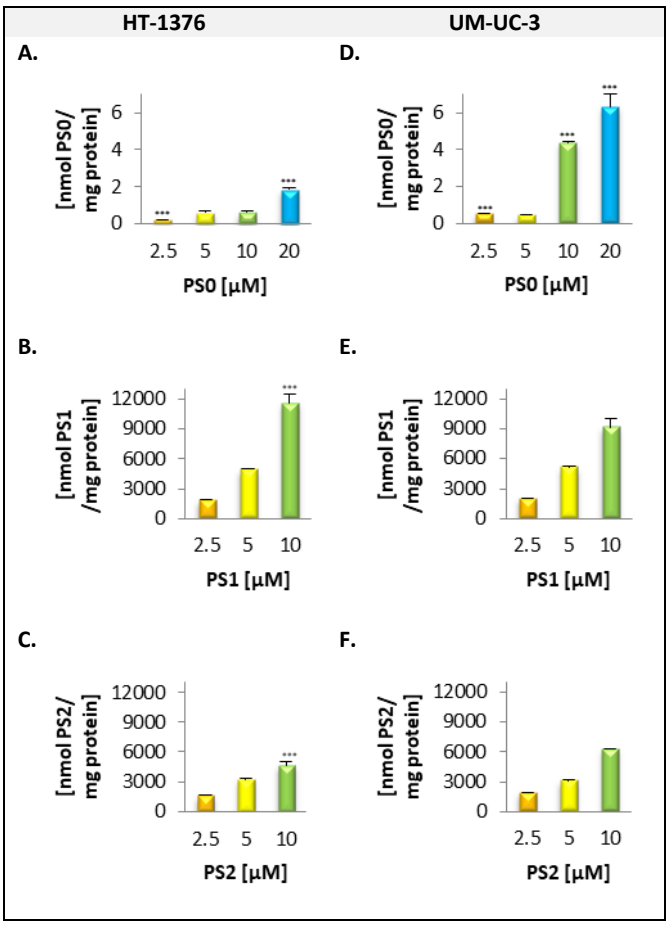

Figure 5. Intracellular uptake of **PS0**, **PS1**, **PS2** (0-10 μM in PBS) by UM-UC-3 and HT-1376 bladder cancer cells. Cells were incubated with **PS** for 4 h and uptake was determined by fluorescence spectroscopy. Data are means ± s.e.m. of at least three independent experiments performed in triplicates. *P < 0.05, **P < 0.01, ***P < 0.001 compared to the PS uptake by UM-UC-3 cancer cells, using Student's *t* test.

Next, the uptake of **MSNP-PS0, MSNP-PS1, MSNP-PS2**, **MSNR-PS1**, and **MSNR-PS2** was evaluated by fluorescence spectroscopy (**Figure 6**) after incubating UM-UC-3 and HT-1376 bladder cancer cells in dark condition with different concentrations of new NPs (0-20 μM of PS in cell medium).

Uptake studies were performed by incubating cancer cells with PS nanoformulations overnight. When the cells were incubated overnight with medium containing NPs solutions there was uptake dependent on the concentration of PS and shape of the NPs but not on the cell line (which was observed with free PSs). Interestingly, the uptake of **MSNP-PS1** was almost three times lower when compared with the uptake of **MSNR-PS1**. On the other hand, although the uptake of **MSNP-PS2** and **MSNR-PS2** by HT-13-76 cells was similar, UM-UC-3 cells displayed a tendency to increase the uptake of **MSNP-PS2**. The presented results suggested that the aspect ratio of MSNPs could not be considered in these studies as a sole parameter to explain cellular uptake results. These studies pointed out that besides the shape of NPs, their chemistry (e.g. concentration of PS on the surface of NPs) and the type of cancer cells are crucial factors for predicting the uptake of NPs in cells (**Table 3**).

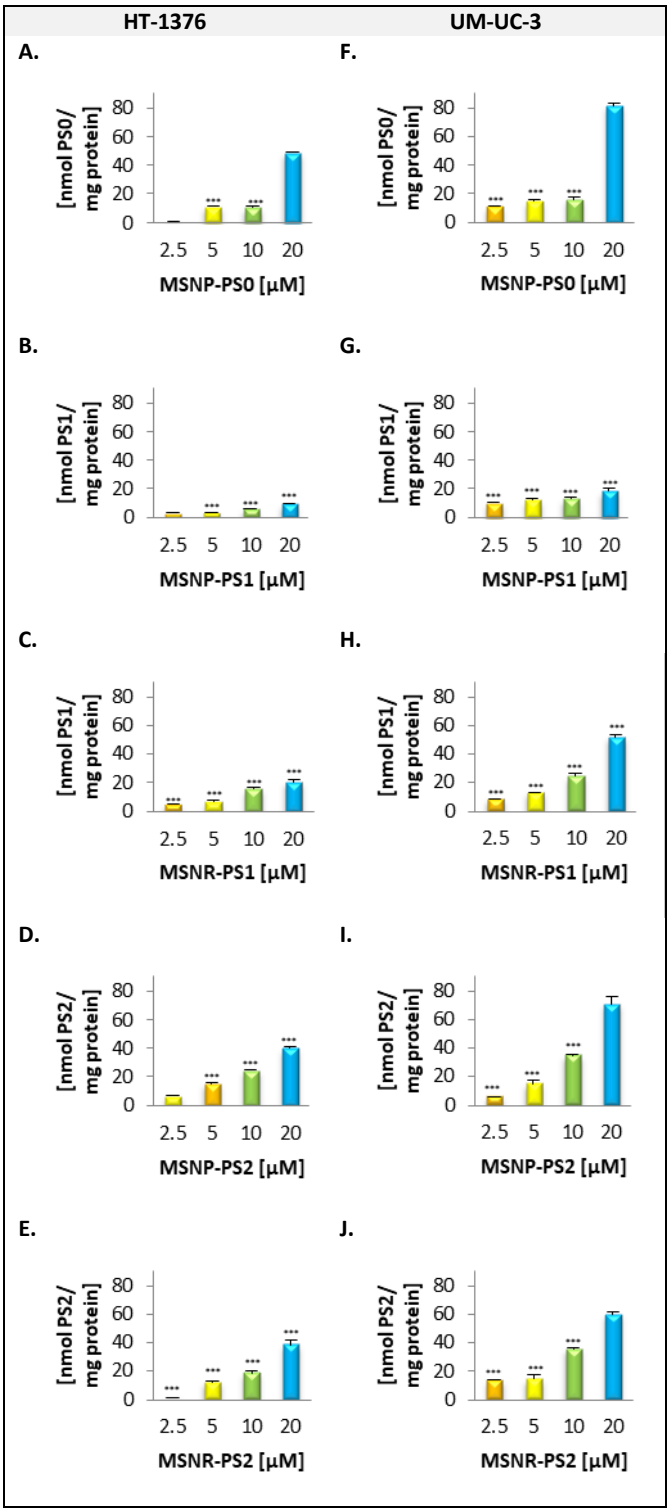

Figure 6. Intracellular overnight uptake of **MSNP-PS0**, **MSNP-PS1**, **MSNR-PS1**, **MSNP-PS2**, and **MSNR-PS2** (0-20 μM of PS in RPMI medium) by UM-UC-3 and HT-1376 bladder cancer cells. Data are means ± s.e.m. of at least three independent experiments performed in triplicates. *P < 0.05, **P < 0.01, ***P < 0.001 compared to the NP uptake by UM-UC-3 cancer cells, using Student's *t* test.

The comparison between the amount of PS on the surface of NPs and the corresponding cell uptake value shows that there is an inverse trend relating to this data, i.e. as the amount of PS per mg of NP increases, there is a decrease in the cell uptake (**Table 3**, **Scheme 2**).

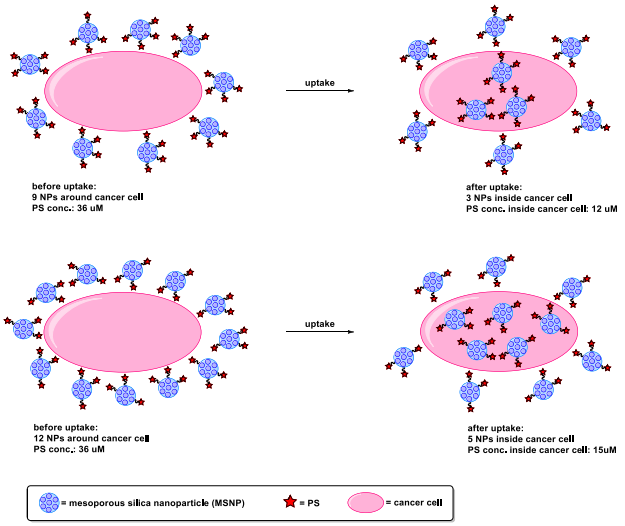

Scheme 2. Schematic representation of suggested uptake process in cancer cells which is in inverse proportion to the concentration of PS on the surface of NP per mg of NP. The same mechanism is proposed for MSNPs and MSNRs.

In the present uptake studies, although the same amount of PS was used, the nanoformulations had different amounts of PS on their surfaces, thus different amounts of NPs were used in the experiments. When the concentration of PS on the NPs' surface was higher, the smaller was the amount of NPs (in mg) taken into the experiment resulting in a smaller uptake. In conclusion, the uptake depends not only on the concentration of PS on the surface of NPs but also on the amount of NPs (in mg or numbers of NPs).

Furthermore, it was observed that the uptake of all new nanoformulations was higher in UM-UC-3 cancer cells (with a high level of galectin-1) when compared with HT-1376 cells (with a high level of GLUT1 protein). This could be a result of a better delivery process of MSNPs and MSNRs in UM-UC-3 than in HT-1376 cells. Interestingly, **MSNP-PS0** was the only sample that accumulated better in both cancer cell lines than the corresponding non-immobilized Por (**Figures 7**, **8**). The uptake of these sphere-shaped particles was ten times better in cancer cells when compared to free **PS0**. **MSNP-PS0** (117 ± 16 nm) had the tendency to accumulate in cancer cells much more than smaller molecules of **PS0**.

From uptake results, it could be concluded that the cell uptake depends not only on the shape of nanocarriers but also on the type of PS, the concentration of PS on the surface of NPs, and the amount of NPs employed (in mg or numbers of NPs).

Dark toxicity and phototoxicity

The dark toxicity of **PS0**, **PS1**, **PS2** and its corresponding nanoformulations (**MSNP-PS0, MSNP-PS1, MSNP-PS2** and **MSNR-PS1, MSNR-PS2**) was evaluated using the well-known MTT assay (**Figures SI 10**, **11**) in UM-UC-3 and HT-1376 bladder cancer cells. This colorimetric assay uses the ability of viable cells to reduce yellow 3-[4,5-dimethylthiazol-2-yl]-2,5-diphenyl-tetrazolium bromide (MTT), to purple formazan. Thus, it is a straightforward tool to determine cell metabolic activity. After overnight incubation of cancer cells (in dark) with NPs (0-20 µM of PS in RPMI medium) or 4 h incubation with PSs (0-10 µM in PBS buffer), none of the PSs or new NPs induced dark toxicity in cancer cells. This outcome is crucial in the PDT concept since the ideal therapeutic drug should not show cytotoxicity until photoactivation.

Following the confirmation of the uptake and non-dark toxicity of PSs and their new nanoformulations in UM-UC-3 and HT-1376 bladder cancer cells, their toxicity after light irradiation was evaluated using the MTT assay (**Figures 7**, **8**).

In this study, UM-UC-3 and HT-1376 bladder cancer cells were incubated with PSs (0-10 µM in PBS buffer) for 4 h or with NPs (0-20 µM of PS in RPMI medium) overnight and then irradiated with an optical fiber emitting white light for 40 min (8.4 mW/cm^2). No cytotoxicity was observed in the sham irradiated, or left untreated (cells incubated in the absence of NPs).

When the cells were incubated for 4 h in PBS containing PSs (0-10 µM in PBS buffer) there was phototoxicity dependent on the concentration of the PSs (**Figure 7**). **PS1** and **PS2** led to higher phototoxicity in both cancer cells than **PS0** sample. This could be explained by the fact that these two PSs with sugar units presented much better uptake properties in HT-1376 and UM-UC-3 cancer cells compared to **PS0**. **PS1** and **PS2** presented slightly higher phototoxicity in UM-UC-3 cancer cells than in HT-1376 cancer cells.

After UM-UC-3 and HT-1376 bladder cancer cells were incubated overnight in medium with NPs (0-20 µM of PS) there was phototoxicity dependent on the concentration of the PSs(**Figure 8**). Although all new NPs induced phototoxicity in UM-UC-3 and HT-1376 bladder cancer cells in a concentration-dependent manner, the overall phototoxicity was higher with PSs than with NP formulations.

In general, the phototoxicity was higher with MSNPs than with MSNRs (**Table 3**). All NPs presented higher phototoxicity in UM-UC-3 cancer cells than in HT-1376 cancer cells. Which could be the result of better uptake observed in these cell lines (**Figure 8**). Although the best cellular uptake was observed for **MSNP-PS2** in both UM-UC-3 and HT-1376 bladder cancer cells, **MSNP-PS1** with the lowest uptake results presented the highest phototoxicity in the same cancer cells lines (**Table 3**).

There is a clear relationship between the uptake behavior and phototoxicity results in terms of cell line. For all nanovehicles, a higher uptake was observed in UM-UC-3 than in HT-1376 cancer cells. The same behavior was spotted during phototoxicity studies. The phototoxicity was higher in UM-UC-3 than in HT-1376 cancer cells. Moreover, MSNPs showed higher phototoxicity in both cancer cells compared to MSNRs.

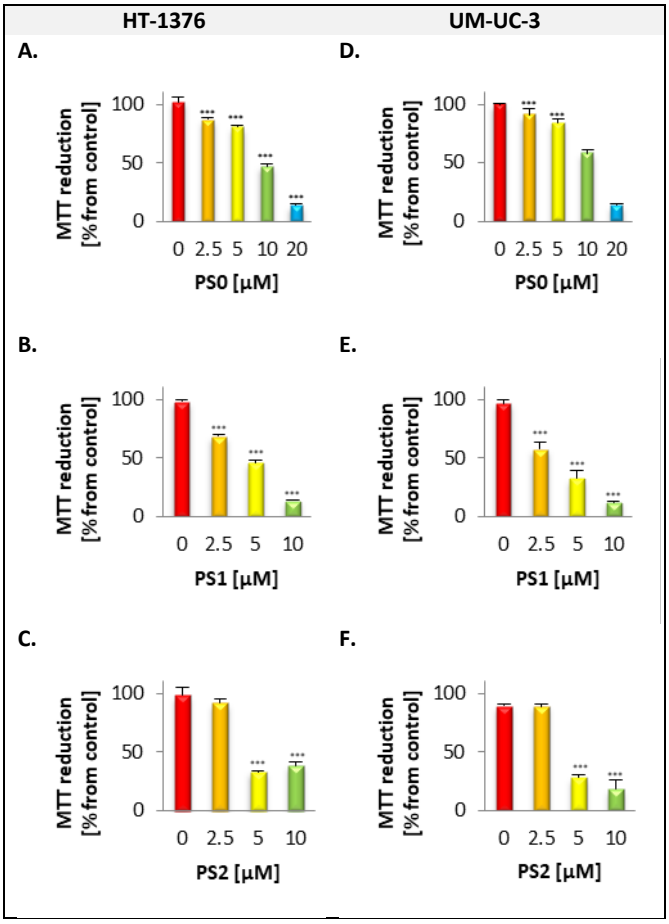

Figure 7. Phototoxicity of **PS0** (0-20 μM), **PS1** (0-10 μM), **PS2** (0-10 μM) determined 24 h after PDT treatment using the MTT assay. Photodynamic irradiation was carried out with white light at 8.4 mW/cm-2 for 40 min. The percentage of cytotoxicity was calculated relatively to control cells (cells incubated with PBS and then irradiated). Data are means ± s.e.m. of at least three independent experiments performed in triplicates. *P < 0.05, **P < 0.01, ***P < 0.001 compared to MTT reduction in control cells, using Student's *t* test.

Although **MSNP-PS1** showed the lowest cellular uptake among other nanocarriers tested in both cancer cell lines, these NPs produced the highest phototoxic effect in both cancer cells. These results suggested that other factors are also relevant in the phototoxic effect of these NPs. For example, **MSNP-PS1** has a higher concentration of PS on the surface of NPs [25 nmol of PS/mg of NP] comparing to the other tested nanomaterials, which eventually could result in better production of ROS. Other factors, such as subcellular localization of NPs or PSs also play a role in the outcome of PDT.[37] The subcellular localization of NPs depends, for example, on the chemical nature of the NPs, particle size and shape, surface charge, targeting ligands, exposure duration as well as cell type.[38] Thus, further studies are required to investigate the parameters that guide the PDT effect of these new NPs.

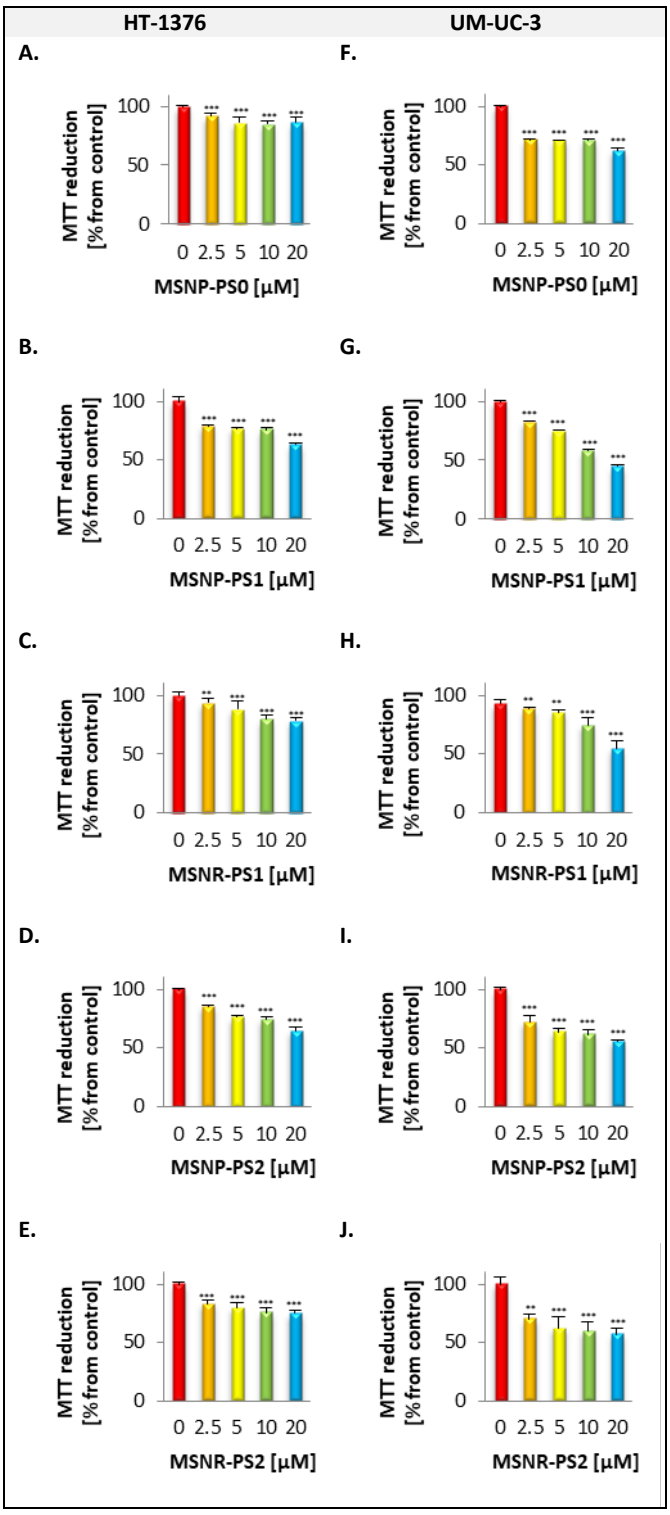

Figure 8. Phototoxicity of **MSNP-PS0, MSNP-PS1, MSNP-PS2** and **MSNR-PS1, MSNR-PS2** (0-20 μM of PS) determined 24 h after PDT treatment using the MTT assay. Photodynamic irradiation was carried out with white light at 8.4 mW/cm-2 for 40 min. The percentage of cytotoxicity was calculated relatively to control cells (cells incubated with medium and then irradiated). Data are means ± s.e.m. of at least three independent experiments performed in triplicates. *P < 0.05, **P < 0.01, ***P < 0.001 compared to MTT reduction in control cells, using Student's *t* test.

Table 3. Relation between the concentration of PS on the surface of NPs and its cellular uptake behavior with phototoxicity results (*the concentration is presented as the concentration of PS in the NP; **the uptake is presented for 20 μM of PS into each experiment; ***the phototoxicity is presented after 30 min of light irradiation as a MTT reduction (% from control)).

NP name	Concentration of PS [nmol of PS/mg of NP]*	Uptake [nmol PS/mg protein]**		Phototoxicity [%]***	
		HT-1376	UM-UC-3	HT-1376	UM-UC-3
MSNP-PS1	25.0	9.8	18.7	37.2	55.1
MSNR-PS1	22.9	20.5	51.8	21,9	45.2
MSNP-PS2	19.8	39.9	70.6	35,5	44.8
MSNR-PS2	22.6	38.3	60.1	25.1	42.8

Although all new NPs induced phototoxicity in UM-UC-3 and HT-1376 bladder cancer cells in a concentration-dependent manner, the overall phototoxicity was higher with free PSs than with NPs. Concerning the phototoxicity of all new nanovehicles, a second light irradiation treatment could increase *in vitro* photodynamic efficacy, as was already demonstrated by us.[39] In the period between single and repeated irradiation, NPs could accumulate in different cellular organelles, which could enhance phototoxicity in both cancer cell lines.

Conclusions

The resulting new nanocarriers were fully described and their properties as new third-generation PSs for PDT against two bladder cancer cell lines, HT-1376 and UMUC-3 were proved. We revealed that MSNPs not only produced more $^1O_2$ during singlet oxygen study but also have higher phototoxicity in both cancer cell lines compared to MSNRs. The final results suggested that our new sphere-shaped nano-systems could be successfully used in PDT of bladder cancer which is the fourth most commonly diagnosed cancer[40] with a high rate of recurrence. Further advances towards improving the therapeutic efficacy of PDT treatment by these NPs and understanding the parameters that guide their PDT effect are under research.

Author Contributions

W.B.: synthesis and characterization of NPs, singlet oxygen generation study, *in vitro* assays, writing—original draft preparation, review, and editing; **P. M. R. P.**: *in vitro* assays, writing—review and editing; **R. Fernandes, T. Trindade**, **T. Torres** and **J. Tomé**: supervision, writing—review and editing.

Conflicts of interest

There are no conflicts to declare.

Acknowledgements

Thanks are due to FCT/MEC for the financial support to LAQV-REQUIMTE (UIDB/50006/2020), CICECO-Aveiro Institute of Materials (UIDB/50011/2020), CIBB (UIDB/04539/2020 and UIDP/04539/2020) and CQE (UIDB/00100/2020) research units, through national funds and where applicable cofinanced by the FEDER, within the PT2020 Partnership Agreement. The work was also supported by the Spanish MINECO (PID2020-116490GB-I00, Porphyrinoids), MINECO/ERA-NET (PCIN-2017-042/EuroNanoMed2017-191, TEMPEAT), and Portuguese COMPETE (POCI-01-0145-FEDER-007440). IMDEA Nanociencia also acknowledges support from the 'Severo Ochoa' Programme for Centres of Excellence in R&D (MINECO, Grant SEV-2016-0686). We further wish to thank the Seventh Framework Programme (FP7-People-2012-ITN) for funding the SO2S project (grant agreement number: 316975). The authors also acknowledge FCT for the doctoral research fellowship SFRH/BD/85941/2012 (to PMRP).

Notes and references

1. Railkar, R.; Agarwal, P. K., Photodynamic Therapy in the Treatment of Bladder Cancer: Past Challenges and Current Innovations. *European Urology Focus* **2018,** *4* (4), 509-511.
2. (a) Bonnett, R., Photosensitizers of the porphyrin and phthalocyanine series for photodynamic therapy. *Chem. Soc. Rev.* **1995,** *24* (1), 19-33; (b) Henderson, B. W.; Dougherty, T. J., How does photodynamic therapy work? *Photochem. Photobiol.* **1992,** *55* (1), 145-157; (c) Dolmans, D. E. J. G. J.; Fukumura, D.; Jain, R. K., Photodynamic therapy for cancer. *Nat. Rev. Cancer* **2003,** *3* (5), 380-387; (d) Macdonald, I. J.; Dougherty, T. J., Basic principles of photodynamic therapy. *J. Porphyrins Phthalocyanines* **2001,** *05* (02), 105-129.
3. Lucky, S. S.; Soo, K. C.; Zhang, Y., Nanoparticles in Photodynamic Therapy. *Chemical Reviews* **2015,** *115* (4), 1990-2042.
4. Dolmans, D. E. J. G. J.; Fukumura, D.; Jain, R. K., Photodynamic therapy for cancer. *Nature Reviews Cancer* **2003,** *3* (5), 380-387.
5. Agostinis, P.; Berg, K.; Cengel, K. A.; Foster, T. H.; Girotti, A. W.; Gollnick, S. O.; Hahn, S. M.; Hamblin, M. R.; Juzeniene, A.; Kessel, D.; Korbelik, M.; Moan, J.; Mroz, P.; Nowis, D.; Piette, J.; Wilson, B. C.; Golab, J., Photodynamic Therapy of Cancer: An Update. *A Cancer Journal for Clinicians* **2011,** *61*, 250-281.
6. (a) Chatterjee, D. K.; Fong, L. S.; Zhang, Y., Nanoparticles in photodynamic therapy: An emerging paradigm. *Advanced Drug Delivery Reviews* **2008,** *60* (15), 1627-1637; (b) Idris, N. M.; Gnanasammandhan, M. K.; Zhang, J.; Ho, P. C.; Mahendran, R.; Zhang, Y., In vivo photodynamic therapy using upconversion nanoparticles as remote-controlled nanotransducers. *Nature Medicine* **2012,** *18*, 1580-1586; (c) Qian, H. S.; Guo, H. C.; Ho, P. C.-L.; Mahendran, R.; Zhang, Y., Mesoporous-Silica-Coated Up-Conversion Fluorescent Nanoparticles for Photodynamic Therapy. *Small* **2009,** *5* (20), 2285-2290.
7. (a) Couleaud, P.; Morosini, V.; Frochot, C.; Richeter, S.; Raehma, L.; Durand, J.-O., Silica-based nanoparticles for photodynamic therapy applications. *Nanoscale* **2010,** *2*, 1083-1095; (b) Kobayashi, H.; Watanabe, R.; Choyke, P. L., Improving Conventional Enhanced Permeability and Retention (EPR) Effects; What Is the Appropriate Target? *Theranostics* **2014,** *4* (1), 81-89; (c) Maeda, H., Tumor-

Selective Delivery of Macromolecular Drugs via the EPR Effect: Background and Future Prospects. *Bioconjugate Chemistry* **2010,** *21* (5), 797-802.

8. Kresge, C. T.; Leonowicz, M. E.; Roth, W. J.; Vartuli, J. C.; Beck, J. S., Ordered mesoporous molecular sieves synthesized by a liquid-crystal template mechanism. *Nature* **1992,** *359* (6397), 710-712.

9. Vallet-Regi, M.; Rámila, A.; del Real, R. P.; Pérez-Pariente, J., A New Property of MCM-41: Drug Delivery System. *Chemistry of Materials* **2001,** *13* (2), 308-311.

10. (a) Slowing, I. I.; Trewyn, B. G.; Giri, S.; Lin, V. S. Y., Mesoporous Silica Nanoparticles for Drug Delivery and Biosensing Applications. *Advanced Functional Materials* **2007,** *17* (8), 1225-1236; (b) Muñoz, B.; Rámila, A.; Pérez-Pariente, J.; Díaz, I.; Vallet-Regí, M., MCM-41 Organic Modification as Drug Delivery Rate Regulator. *Chemistry of Materials* **2003,** *15* (2), 500-503.

11. Tang, L.; Cheng, J., Nonporous silicana noparticles for nanomedicine application. *Nano Today* **2013,** *8*, 290-312.

12. Yang, Y.; Yu, C., Advances in silica based nanoparticles for targeted cancer therapy. *Nanomedicine: Nanotechnology, Biology and Medicine* **2016,** *12* (2), 317-332.

13. (a) Dawidczyk, C. M.; Kim, C.; Park, J. H.; Russell, L. M.; Lee, K. H.; Pomper, M. G.; Searson, P. C., State-of-the-art in design rules for drug delivery platforms: Lessons learned from FDA-approved nanomedicines. *Journal of Controlled Release* **2014,** *187*, 133-144; (b) Pillai, G., Nanomedicines for Cancer Therapy: An Update of FDA Approved and Those under Various Stages of Development. *SOJ Pharmacy & Pharmaceutical Sciences* **2014,** *1*, 1-13; (c) Gopalakrishna Pillai; Ceballos-Coronel, M. L., Science and technology of the emerging nanomedicines in cancer therapy: A primer for physicians and pharmacists. *SAGE Open Medicine* **2013,** *1*, 1.

14. Jafari, S.; Derakhshankhah, H.; Alaei, L.; Fattahi, A.; Varnamkhasti, B. S.; Saboury, A. A., Mesoporous silica nanoparticles for therapeutic/diagnostic applications. *Biomedicine & Pharmacotherapy* **2019,** *109*, 1100-1111.

15. Chithrani, B. D.; Chan, W. C. W., Elucidating the Mechanism of Cellular Uptake and Removal of Protein-Coated Gold Nanoparticles of Different Sizes and Shapes. *Nano Letters* **2007,** *7* (6), 1542-1550.

16. Florez, L.; Herrmann, C.; Cramer, J. M.; Hauser, C. P.; Koynov, K.; Landfester, K.; Crespy, D.; Mailänder, V., How Shape Influences Uptake: Interactions of Anisotropic Polymer Nanoparticles and Human Mesenchymal Stem Cells. *Small* **2012,** *8* (14), 2222-2230.

17. Zhang, Y.; Tekobo, S.; Tu, Y.; Zhou, Q.; Jin, X.; Dergunov, S. A.; Pinkhassik, E.; Yan, B., Permission to Enter Cell by Shape: Nanodisk vs Nanosphere. *ACS Applied Materials & Interfaces* **2012,** *4* (8), 4099-4105.

18. Huang, X.; Teng, X.; Chen, D.; Tang, F.; He, J., The effect of the shape of mesoporous silica nanoparticles on cellular uptake and cell function. *Biomaterials* **2010,** *31* (3), 438-448.

19. Yang, G.; Gong, H.; Qian, X.; Tan, P.; Li, Z.; Liu, T.; Liu, J.; Li, Y.; Liu, Z., Mesoporous silica nanorods intrinsically doped with photosensitizers as a multifunctional drug carrier for combination therapy of cancer. *Nano Research* **2015,** *8* (3), 751-764.

20. Meng, H.; Yang, S.; Li, Z.; Xia, T.; Chen, J.; Ji, Z.; Zhang, H.; Wang, X.; Lin, S.; Huang, C.; Zhou, Z. H.; Zink, J. I.; Nel, A. E., Aspect Ratio Determines the Quantity of Mesoporous Silica Nanoparticle Uptake by a Small GTPase-Dependent Macropinocytosis Mechanism. *ACS Nano* **2011,** *5* (6), 4434-4447.

21. (a) Figueira, F.; Cavaleiro, J. A. S.; Tomé, J. P. C., Silica nanoparticles functionalized with porphyrins and analogs for biomedical studies. *J. Porphyrins Phthalocyanines* **2011,** *15* (07n08), 517-533; (b) Borzęcka, W.; Trindade, T.; Torres, T.; Tomé, J., Targeting Cancer Cells with Photoactive Silica Nanoparticles. *Current Pharmaceutical Design* **2016,** *22* (39), 6021-6038; (c) Cheng, S.-H.; Lee, C.-H.; Yang, C.-S.; Tseng, F.-G.; Mou, C.-Y.; Lo, L.-W., Mesoporous silica nanoparticles functionalized with an oxygen-sensing probe for cell photodynamic therapy: potential cancer theranostics. *Journal of Materials Chemistry* **2009,** *19* (9), 1252-1257; (d) Tu, H.-L.; Lin, Y.-S.; Lin, H.-Y.; Hung, Y.; Lo, L.-W.; Chen, Y.-F.; Mou, C.-Y., In vitro Studies of Functionalized Mesoporous Silica Nanoparticles for Photodynamic Therapy. *Advanced Materials* **2009,** *21* (2), 172-177; (e) Zhang, R.; Wu, C.; Tong, L.; Tang, B.; Xu, Q.-H., Multifunctional Core-Shell Nanoparticles as Highly Efficient Imaging and Photosensitizing Agents. *Langmuir* **2009,** *25* (17), 10153–10158; (f) Brevet, D.; Gary-Bobo, M.; Raehm, L.; Richeter, S.; Hocine, O.; Amro, K.; Loock, B.; Couleaud, P.; Frochot, C.; Morere, A.; Maillard, P.; Garcia, M.; Durand, J.-O., Mannose-targeted mesoporous silica nanoparticles for photodynamic therapy. *ChemComm* **2009,** (12), 1475–1477; (g) Cheng, S.-H.; Lee, C.-H.; Chen, M.-C.; Souris, J. S.; Tseng, F.-G.; Yang, C.-S.; Mou, C.-Y.; Chen, C.-T.; Lo, L.-W., Tri-functionalization of mesoporous silica nanoparticles for comprehensive cancer theranostics-the trio of imaging, targeting and therapy. *Journal of Materials Chemistry* **2010,** *20* (29), 6149-6157.

22. Guo, X.; Guo, B.; Sun, X.; Zhang, Q.; Shi, T., Preparation of Novel Silica Nanoparticles with Controllable Fluorescence Intensity from Porphyrin-Bridged Silsesquioxane. *Chin. J. Chem.* **2011,** *29*, 363-368.

23. Hocine, O.; Gary-Bobo, M.; Brevet, D.; Maynadier, M.; Fontanel, S.; Raehm, L.; Richeter, S.; Loock, B.; Couleaud, P.; Frochot, C.; Charnay, C.; Derrien, G.; Smaïhi, M.; Sahmoune, A.; Morère, A.; Maillard, P.; Garcia, M.; Durand, J.-O., Silicalites and Mesoporous Silica Nanoparticles for photodynamic therapy. *International Journal of Pharmaceutics* **2010,** *402* 221-230.

24. Vivero-Escoto, J. L.; Vega, D. L., Stimuli-responsive protoporphyrin IX silica-based nanoparticles for photodynamic therapy in vitro. *RSC Adv.* **2014,** *4*, 14400–14407.

25. Perrier, M.; Gary-Bobo, M.; Lartigue, L.; Brevet, D.; Morère, A.; Garcia, M.; Maillard, P.; Raehm, L.; Guari, Y.; Larionova, J.; Durand, J.-O.; Mongin, O.; Blanchard-Desce, M., Mannose-functionalized porous silica-coated magnetic nanoparticles for two-photon imaging or PDT of cancer cells. *J. Nanopart. Res.* **2013,** *15*, 1-17.

26. Hayashi, K.; Nakamura, M.; Miki, H.; Ozaki, S.; Abe, M.; Matsumoto, T.; Kori, T.; Ishimura, K., Photostable Iodinated Silica/Porphyrin Hybrid Nanoparticles with Heavy-Atom Effect for Wide-Field Photodynamic/Photothermal Therapy Using Single Light Source. *Adv. Funct. Mater.* **2014,** *24* (4), 503-513.

27. Borzęcka, W.; Pereira, P. M. R.; Fernandes, R.; Trindade, T.; Torres, T.; Tomé, J. P. C., Encapsulation of glycosylated porphyrins in silica nanoparticles to enhance the efficacy of cancer photodynamic therapy. *Materials Advances* **2021**.

28. Hong, S. h.; Choi, Y., Mesoporous silica-based nanoplatforms for the delivery of photodynamic therapy agents. *Journal of Pharmaceutical Investigation* **2018,** *48* (1), 3-17.

29. (a) Cindolo, L.; Benvenuto, G.; Salvatore, P.; Pero, R.; Salvatore, G.; Mirone, V.; Prezioso, D.; Altieri, V.; Bruni, C. B.; Chiariotti, L., Galectin-1 and galectin-3 expression in human bladder transitional-cell carcinomas. *International Journal of Cancer* **1999,** *84* (1), 39-43; (b) Pereira, P. M. R.; Silva, S.; Cavaleiro, J. A. S.; Ribeiro, C. A. F.; Tomé, J. P. C.; Fernandes, R., Galactodendritic Phthalocyanine Targets Carbohydrate-Binding Proteins Enhancing Photodynamic Therapy. *PLoS ONE* **2014,** *9* (4), e95529.

30. (a) Carruthers, A.; DeZutter, J.; Ganguly, A.; Devaskar, S. U., Will the original glucose transporter isoform please stand up! *American Journal of Physiology - Endocrinology And Metabolism* **2009,** *297* (4), E836-E848; (b) Fernandes, R.; Hosoya, K.-i.; Pereira, P., Reactive oxygen species downregulate glucose transport system in retinal

endothelial cells. *American Journal of Physiology - Cell Physiology* **2011,** *300* (4), C927-C936.
31. Chan, H. B. S.; Budd, P. M.; Naylor, T. d., Control of mesostructured silica particle morphology. *Journal of Materials Chemistry* **2001,** *11* (3), 951-957.
32. Carvalho, C. M. B.; Alves, E.; Costa, L.; Tomé, J. P. C.; Faustino, M. A. F.; Neves, M. G. P. M. S.; Tomé, A. C.; Cavaleiro, J. A. S.; Almeida, A.; Cunha, Â.; Lin, Z.; Rocha, J., Functional Cationic Nanomagnet−Porphyrin Hybrids for the Photoinactivation of Microorganisms. *ACS Nano* **2010,** *4* (12), 7133-7140.
33. (a) Chen, X.; Hui, L.; Foster, D. A.; Drain, C. M., Efficient Synthesis and Photodynamic Activity of Porphyrin-Saccharide Conjugates: Targeting and Incapacitating Cancer Cells†. *Biochemistry* **2004,** *43* (34), 10918-10929; (b) Shiho HirohHirohara, S.; Obata, M.; Alitomo, H.; Sharyo, K.; Ando, T.; Yano, S.; Tanihara, M., Synthesis and Photocytotoxicity of S-Glucosylated 5,10,15,20-Tetrakis(tetrafluorophenyl)porphyrin Metal Complexes as Efficient 1O2-Generating Glycoconjugates. *Bioconjugate Chemistry* **2009,** *20*, 944-952; (c) Singh, S.; Aggarwal, A.; Thompson, S.; Tomé, J. P. C.; Zhu, X.; Samaroo, D.; Vinodu, M.; Gao, R.; Drain, C. M., Synthesis and Photophysical Properties of Thioglycosylated Chlorins, Isobacteriochlorins, and Bacteriochlorins for Bioimaging and Diagnostics. *Bioconjugate Chemistry* **2010,** *21*, 2136-2146; (d) Hirohara, S.; Nishida, M.; Sharyo, K.; Obata, M.; Ando, T.; Tanihara, M., Synthesis, photophysical properties and photocytotoxicity of mono-, di-, tri- and tetra-glucosylated fluorophenylporphyrins. *Bioorganic & Medicinal Chemistry* **2010,** *18* (4), 1526-1535; (e) Hirohara, S.; Obata, M.; Alitomo, H.; Sharyo, K.; Ando, T.; Tanihara, M.; Yano, S., Synthesis, photophysical properties and sugar-dependent in vitro photocytotoxicity of pyrrolidine-fused chlorins bearing S-glycosides. *Journal of Photochemistry and Photobiology B: Biology* **2009,** *97* (1), 22-33.
34. (a) Huang, X.; Li, L.; Liu, T.; Hao, N.; Liu, H.; Chen, D.; Tang, F., The Shape Effect of Mesoporous Silica Nanoparticles on Biodistribution, Clearance, and Biocompatibility in Vivo. *ACS Nano* **2011,** *5* (7), 5390-5399; (b) Hao, N.; Yang, H.; Li, L.; Li, L.; Tang, F., The shape effect of mesoporous silica nanoparticles on intracellular reactive oxygen species in A375 cells. *New Journal of Chemistry* **2014,** *38* (9), 4258-4266.
35. Fernández, L.; Borzecka, W.; Lin, Z.; Schneider, R. J.; Huvaere, K.; Esteves, V. I.; Cunha, Â.; Tomé, J. P. C., Nanomagnet-photosensitizer hybrid materials for the degradation of 17β-estradiol in batch and flow modes. *Dyes and Pigments* **2017,** *142*, 535-543.
36. (a) Frey, B. L.; Corn, R. M., Covalent Attachment and Derivatization of Poly(l-lysine) Monolayers on Gold Surfaces As Characterized by Polarization−Modulation FT-IR Spectroscopy. *Analytical Chemistry* **1996,** *68* (18), 3187-3193; (b) Feifel, S. C.; Lisdat, F., Silica nanoparticles for the layer-by-layer assembly of fully electro-active cytochrome c multilayers. *Journal of Nanobiotechnology* **2011,** *9*, 59-59; (c) Suteewong, T.; Sai, H.; Bradbury, M.; Estroff, L. A.; Gruner, S. M.; Wiesner, U., Synthesis and Formation Mechanism of Aminated Mesoporous Silica Nanoparticles. *Chemistry of Materials* **2012,** *24* (20), 3895-3905.
37. (a) Castano, A. P.; Demidova, T. N.; Hamblin, M. R., Mechanisms in photodynamic therapy: part one-photosensitizers, photochemistry and cellular localization. *Photodiagnosis and photodynamic therapy* **2004,** *1* (4), 279-293; (b) Kessel, D., Correlation between subcellular localization and photodynamic efficacy. *Journal of Porphyrins and Phthalocyanines* **2004,** *08* (08), 1009-1014.
38. Liu, C.-G.; Han, Y.-H.; Kankala, R. K.; Wang, S.-B.; Chen, A.-Z., Subcellular Performance of Nanoparticles in Cancer Therapy. *International journal of nanomedicine* **2020,** *15*, 675-704.
39. Pereira, P. M. R.; Silva, S.; Bispo, M.; Zuzarte, M.; Gomes, C.; Girão, H.; Cavaleiro, J. A. S.; Ribeiro, C. A. F.; Tomé, J. P. C.; Fernandes, R., Mitochondria-Targeted Photodynamic Therapy with a Galactodendritic Chlorin to Enhance Cell Death in Resistant Bladder Cancer Cells. *Bioconjugate Chemistry* **2016,** *27* (11), 2762-2769.
40. Siegel, R. L.; Miller, K. D.; Jemal, A., Cancer statistics, 2016. *CA: A Cancer Journal for Clinicians* **2016,** *66* (1), 7-30.

